PCCP

Accepted Manuscript

This is an *Accepted Manuscript*, which has been through the Royal Society of Chemistry peer review process and has been accepted for publication.

Accepted Manuscripts are published online shortly after acceptance, before technical editing, formatting and proof reading. Using this free service, authors can make their results available to the community, in citable form, before we publish the edited article. We will replace this *Accepted Manuscript* with the edited and formatted *Advance Article* as soon as it is available.

You can find more information about *Accepted Manuscripts* in the Information for Authors.

Please note that technical editing may introduce minor changes to the text and/or graphics, which may alter content. The journal's standard Terms & Conditions and the Ethical guidelines still apply. In no event shall the Royal Society of Chemistry be held responsible for any errors or omissions in this *Accepted Manuscript* or any consequences arising from the use of any information it contains.

ROYAL SOCIETY OF CHEMISTRY

www.rsc.org/pccp

Physical Chemistry Chemical Physics RSCPublishing

ARTICLE

Nanocrystal-constructed mesoporous $CoFe_2O_4$ nanowire arrays aligned on flexible carbon fabric as integrated anodes with enhanced lithium storage properties

Cite this: DOI: 10.1039/x0xx00000x

Received 00th January 2012,
Accepted 00th January 2012

DOI: 10.1039/x0xx00000x

www.rsc.org/

Bo Wang, Songmei Li,* Xiaoyu Wu, Bin Li, Jianhua Liu, and Mei Yu

A novel and facile two-step strategy is successfully developed for large-scale fabrication of hierarchical mesoporous $CoFe_2O_4$ nanowire arrays (NWAs) on flexible carbon fabric as integrated anodes for highly efficient and reversible lithium storage. The synthesis involves the co-deposition of uniform bimetallic (Co, Fe) carbonate hydroxide hydrate precursor NWAs on carbon fabric and subsequent thermal transformation to spinel $CoFe_2O_4$ without damaging the morphology. The as-prepared $CoFe_2O_4$ nanowires have unique mesoporous structures, which are constructed by many interconnected nanocrystals with sizes of about 15-20 nm. And typical size of the nanowires is in the range of 70-100 nm in width and up to several micrometers in length. Such a hybrid nanostructure electrode presented here not only simplify the electrode processing, but also promise fast electron transport/collection and ion diffusion, and withstand volume variation upon prolonged charge/discharge cycling. As a result, the binder-free $CoFe_2O_4$/carbon fabric composite exhibits a high reversible capacity of 1185.75 mAh g^{-1} at a current densities of 200 mA g^{-1}, superior rate capability. More importantly, the reversible capacity can retain as high as ~950 mAh g^{-1} and has no obvious decay after 150 cycles.

Introduction

Increasing power and energy demands for next-generation flexible, portable, light-weight and stretchable electronic devices have stimulated extensive efforts to develop matchable flexible energy storage and conversion systems as power sources, such as lithium-ion batteries (LIBs), supercapacitors (SCs), solar cells, etc.[1-3] Among the various energy storage devices, LIBs has been widely used as an attractive power sources for popular mobile devices owing to its high energy density, long cycle life and environmental benignity.[4,5] In order to further facilitate their portability, the flexible LIBs have become state-of-art power sources in the field of flexible, light-weight, bendable and safe operation energy storage devices.[6]

Compared with conventional devices, flexible energy storage and conversion devices are not limited by bulky design and configuration limitations.[7] Recently, a number of studies, initiatives and products have been reported and proposed to realize mechanical fiexibility of batteries by making each component more flexible in order to make them more suitable for practical applications.[6] Flexible electrode materials are core components for constructing flexible LIBs. To fabricate flexible electrodes, the new substrates must meet such requirements as mechanical property, flexibility, and environmentally friendliness. To date, the conductive films and textiles formed by CNTs, reduced graphene oxide (rGO) and conducting polymers have been widely fabricated and used as conducting substrates to load electroactive materials.[8,9] However, the fabrication of films of CNTs and rGO with large area is difficult and costly. Therefore, textile-based energy storage designs are mostly adopted by researchers, as they have advantages over polymer films and paper, since they are flexible, bendable, do not kink, and recover their shape.[10-12] Particularly, carbon fabric (CF) has been studied as an ideal conductive substrate for directly growing active material due to its unique properties including high electrical conductivity, low-weight, superior mechanical flexibility and low cost, which can fabricate different types flexible SCs or LIBs.[13-15]

To further improve the energy density of LIBs, binary transitional-metal oxides (TMOs) have been extensively conceived as a promising cost-effective and scalable alternative

Key Laboratory of Aerospace Advanced Materials and Performance of Ministry of Education, School of Materials Science and Engineering, Beihang University, Beijing, 100191, China.

E-mail: songmei_li@buaa.edu.cn; Fax: +86-10-82317103; Tel: +86-10-82317103

Electronic supplementary information (ESI) available. See DOI:

Physical Chemistry Chemical Physics Accepted Manuscript

anode materials for LIBs since they offer several advantages, including their high specific/volumetric capacity, high stability and low cost.[16-18] Among these candidates, spinel ferrites, in particular $CoFe_2O_4$, has drawn particular attention because of its much higher theoretical capacity (916 mAh g^{-1}) than that of commercial used graphite (372 mAh g^{-1}), as well as non-toxicity and natural abundance.[19-21] Nevertheless, $CoFe_2O_4$-based anodes also suffer from rapid decay in capacity due to the intrinsically drastic volume changes during the charge/discharge process, which is commonly observed in TMOs-based electrodes.[22-24] Strategies have been proposed to improve the lithium storage capability of TMOs-based electrodes, one effective strategy relies on the establishment of arrayed and integrated 1D architectures with a robust adhesion onto conductive substrates for LIBs anodes, which are all expected to promote the electrochemical processes and maintain the good structural integration.[25-26] Compared to the conventional two-dimensional (2D) thin-film electrode, One dimensional (1D) nanostructure arrays on conductive substrates exhibit great advantages to be used as electrodes for LIBs: (1) The establishment of arrayed and integrated 1D architectures with a robust adhesion to substrate provides a much larger surface-to-volume ratio and a shorten Li-ion diffusion length of 1D nanostructure arrays with respect to the bulk counterparts. (2) The interval space formed between neighboring nanostructures can make easy diffusion of liquid electrolyte to the nanostructured surface, ultimately improving the cycling stability of electrodes. and (3) The additive and binder-free electrode can be effectively improved the overall energy storage capacity by individual nanostructure participates in electrochemical reactions.[27-31] Therefore, it is envisioned that advances in LIBs technology can be achieved by combining both integrated flexible electrode design and porous structure with low-dimensional building blocks in a complete electrode configuration.

Here, we present the rational design and fabrication of a novel and efficient nanoarchitecture, mesoporous $CoFe_2O_4$ nanowire arrays (NWAs) directly integrated onto the surface of flexible carbon fabric, which can be directly applied as self-supported 3D anodes for LIBs. The as-synthesized mesoporous $CoFe_2O_4$ nanowires consist of numerous highly crystalline nanoparticles, leaving a large number of mesopores to increase the electrode-electrolyte interfacial area and alleviate the volume change during the charge/discharge process. When evaluated as binder-free anode materials for LIBs, the $CoFe_2O_4$/carbon fabric composite exhibits high reversible capacity, superior rate capability and cycling performance.

Experimental

Growth of $CoFe_2O_4$ NWAs on carbon fabric

All chemicals (supplied by Beijing Chemical Co.,Ltd.) used were analytical grade and used without further purification. $CoFe_2O_4$ NWAs/carbon fabric electrodes were synthesized by using a simple hydrothermal method followed by a thermal treatment. Prior to deposition, a piece of carbon fabric (CF; ca. 5 cm × 3.5 cm) was pretreated by rinsed with acetone, deionized water, and absolute ethanol for 15 min, respectively. After drying at 60 □ for 5 h, the weight of each treated CF piece was recorded. In a typical process, 6 mmol of $Fe(NO_3)_3$, 3 mmol of $Co(NO_3)_2$, 16 mmol of NH_4F, and 30 mmol of urea were dissolved in 90 mL deionized water to form a transparent pink solution by constant stirring, and then transferred into a 100 mL polytetrafluoroethylene (PTFE) Teflon-lined stainless steel autoclave. Two pieces of treated CF was immersed in the reaction solution and kept at 120 □ for 6 h to allow the hydrothermal growth of the CoFe-precursor NWAs. After that, the autoclave was cooled down to room temperature naturally, and the CF covered with CoFe-precursor NWAs was removed from the growth solution, rinsed several times with deionized water and absolute ethanol, followed by drying at 60 ℃ for 8 h. The precipitate in the solution was also collected and washed by centrifugation for several times using deionized water and absolute ethanol before drying at 60 ℃ for 8 h. Finally, the samples were put in a quartz tube and calcined under the protection of argon gas ambient at 350 ℃ for 3 h at a rate of 2 □ min^{-1} to obtain well defined crystallized $CoFe_2O_4$ NWAs, and then cooled down to room temperature gradually.

Characterization

The crystallographic structures of the materials were determined by a powder X-ray diffraction system (XRD, Rigaku D/max 2200PC) equipped with Cu Kα radiation (λ=0.15418 nm). The morphologies, chemical compositions, and the microstructures of the products were characterized by field-emission scanning electron microscope (FE-SEM, JEOL JSM-7500F) equipped with an energy dispersive X-ray spectrometry (EDS), transmission electron microscope (TEM, JEOL JEM-2100F), and X-ray photoelectron spectroscope (XPS, AXIS UTLTRADLD equipped with a dual Mg Ka-Al Ka anode for photoexcitation). The N_2 adsorption-desorption were determined by BET measurements using an ASAP-2010 surface area analyzer.

Electrochemical Measurements

The electrochemical properties of the as-prepared products were measured using CR2025-type coin cells assembled in an argon-filled glove box. For the coin-cell assembly, the $CoFe_2O_4$/carbon fabric composite were punched in the form of 11 mm diameter disks, and then used directly as the working electrode without any conductive additive and polymer binder. The loading density of the active material on the electrodes was about 1～1.1 mg cm^{-2}. A metallic lithium foil served as both the counter electrode and the reference electrode, a polypropylene (PP) microporous film (Celgard 2400) was used as the separator, and a solution of 1 M $LiPF_6$ dissolved in ethylene carbonate/dimethyl carbonate (EC:DMC=1:1 v/v) was used as electrolyte.

For the comparative study of electrochemical performance, the $CoFe_2O_4$ powder was also formed into working electrodes. The pasted electrode was fabricated by coating an N-

Physical Chemistry Chemical Physics Accepted Manuscript

 This journal is © The Royal Society of Chemistry 2015

methylpyrrolidinone (NMP) slurry composed of 80 wt.% active materials ($CoFe_2O_4$ powder), 10 wt.% poly(vinylidene fluoride) (PVDF) and 10 wt.% acetylene black on copper foil current collectors followed by drying at 50 ℃ in vacuum oven for 12 h.

The galvanostatic charge/discharge and cyclic voltammetry (CV) measurements were carried out on a CT2001A LAND Cell test system and a multichannel Arbin Instruments BT 2000 (USA) unit in the voltage range of 0.005-3.0 V at room temperature (25±1□). Electrochemical impedance spectroscopy (EIS) measurements were performed in the frequency range from100 kHz to 0.01 Hz on a PARSTRAT 2273 electrochemical workstation under AC stimulus with a potential amplitude of 5 mV. Areal capacity values were calculated based on the area of the working electrode.

Results and discussion

The fabrication processes and the resulting novel electrode architectures developed in this work are schematically illustrated in Scheme 1. The fabrication included two key steps. In the first step, well defined CoFe-precursor NWAs can be easily grown on the highly flexible carbon fabric under hydrothermal condition, in which the whole nucleation-growth process of the CoFe-precursor NWAs proceeded in reaction solution. In the second step, the $CoFe_2O_4$ NWAs/carbon fabric composites can be obtained with well-retained morphology by thermal decomposition of the as-prepared CoFe-precursor NWAs/carbon fabric composites under the protection of argon gas ambient at 350 □ for 3h.

The crystallographic structure of the as-prepared $CoFe_2O_4$/carbon fabric composite were determined from the XRD pattern in Fig. 1a. Fig. 1a shows the XRD patterns of the carbon fabric, annealed products and the standard XRD pattern of cubic CFO. The XRD patterns of carbon fabric display a obvious graphite (002) reflection at 26.21°.[32] With the exception of the reflections owing to carbon fabric, all peaks in the XRD patterns of $CoFe_2O_4$ NWAs/carbon fabric composite can be indexed to face-centered cubic spinel $CoFe_2O_4$ (spacegroup: Fd3m, JCPDS card no. 22-1086).[33,34] No other additional diffraction peaks from possible impurities are

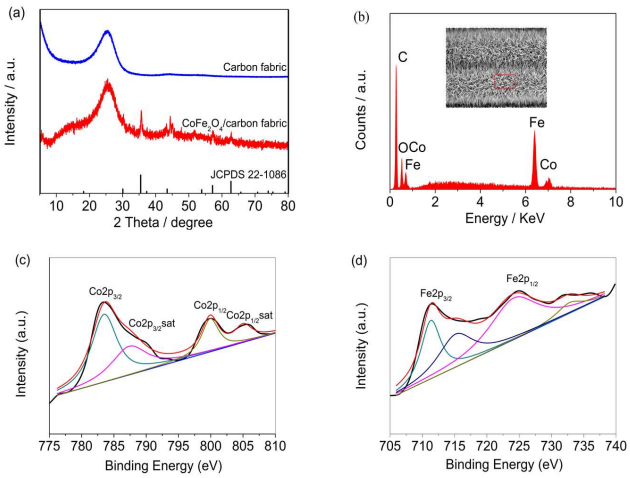

Fig. 1 (a) XRD patterns of carbon fabric, and $CoFe_2O_4$ NWAs/carbon fabric composite, and the standard XRD pattern of cubic CFO. (b) The EDS microanalysis on selected areas. (c) Co2p and (d) Fe2p XPS spectra of $CoFe_2O_4$/carbon fabric composite.

observed, indicating that the CoFe-precursors was converted to crystalline $CoFe_2O_4$ completely. In order to eliminate the influence of the carbon fabric, the collected powders in the same reaction system were also checked by XRD and the corresponding XRD pattern is shown in Fig. S1 (Supporting Information), where all the diffraction peaks can be indexed to pure spinel $CoFe_2O_4$, further confirming the formation of the pure product. Also, the EDS spectrum (Fig. 2b) demonstrates the presence of Fe, Co, C, and O elements in the as-prepared $CoFe_2O_4$/carbon fabric composites, consisting with the XRD results. The elemental composition and oxidation states of the $CoFe_2O_4$/carbon fabric composite are further characterized by X-ray photoelectron (XPS). The survey spectrum (Fig. S2, Supporting Information) indicates the presence of Co, Fe, O, and C elements, and the absence of other impurities. The Co 2p and Fe 2p XPS spectra were fitted by using a Gaussian fitting method (Fig. 1c and d). From the Co2p core level spectrum in Fig. 1c, it was found that four obvious peaks appeared. The first

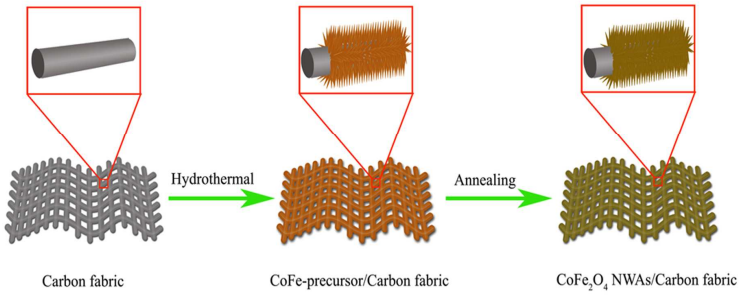

Scheme 1 Schematic illustration of the synthesis of $CoFe_2O_4$ NWAs/carbon fabric composites.

Physical Chemistry Chemical Physics Accepted Manuscript

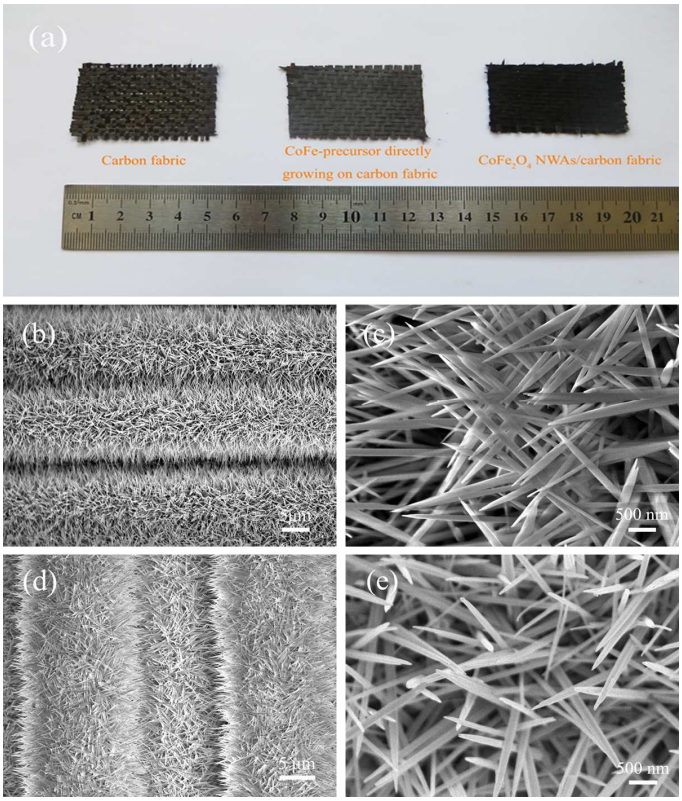

Fig. 2 (a) Photographs of the primitive carbon fabric, before and after annealing treatment by coating with active materials. (b) Low and (c) higher magnification SEM images of the CoFe-precursor NWAs/carbon fabric composite, showing all nanowires completely surrounding the carbon microfiber cores. (d) Low and (e) higher magnification SEM images of the crystalline $CoFe_2O_4$ NWAs/ carbon fabric composite.

two characteristic peaks with binding energies of around 783.3 and 787.7 eV can be ascribed to Co $2p_{3/2}$ and its shake-up satellites, respectively. While the other two peaks with higher binding energies of around 799.7 and 805.5 eV are attributed to Co $2p_{1/2}$ and its shake-up satellite. The presence of the satellite peaks at the higher binding energy of the major signals confirms the chemical state of Co^{2+}.[35-37] In addition, XPS peaks of Fe 2p located at 711.4 and 724.7 eV should be assigned to the spectra of Fe $2p_{3/2}$ and Fe $2p_{1/2}$ (Fig. 1d). The strong spin-orbit separation of ca. 13.3 eV between two major signals is characteristic of Fe^{3+}.[21,38-39] The XPS results confirm that the valence of Co and Fe elements are +2 and +3, respectively.

Fig. 2a shows optical images of the primitive carbon fabric, before and after annealing treatment by coating with active materials. The obvious color change and the final uniform color of the carbon fabric indicate the uniform coating of $CoFe_2O_4$ NWAs samples. The as-fabricated device was lightweight and so highly flexible that it can be even twisted and folded without any detriment of the structural integrity (Fig. S3, Supporting Information). The morphology of the different product was examined with scanning electron microscopy (SEM). The individual carbon fiber of the as-received carbon fabric has a smooth surface and a diameter of about 7 μm (Fig. S4, Supporting Information). Fig. 2b-c show the SEM images at different magnifications of the products after hydrothermal reaction, where uniform hierarchical nanowires arrays of the CoFe-precursors were successfully grown on the entire carbon fabric. Fig. 2d-e show the SEM images of the products after calcination of the hydrothermally grown product under the protection of argon gas ambient at 350□ for 3 h. An enlarged view (Fig. 2e) provides the evidence that the nanowire morphology and the array feature of the naowires are perfectly retained after the annealing conversion. The diameter of the nanowires was reduced a little because of the calcination effects at high temperature. Typical nanowires are several micrometers in length and 70-100 nm in diameter. The presence of $CoFe_2O_4$ is further confirmed by elemental mappings of the composites, as shown in Fig. 3a-e. It can be seen that the cobalt, iron, oxygen, and carbon elements are distributed uniformly in the $CoFe_2O_4$/carbon fabric composites. The porous feature of as-prepared $CoFe_2O_4$/carbon fabric composite is further characterized by Brunauer-Emmert-Teller (BET) analysis. From the Nitrogen isothermal adsorption-desorption isotherm, a unimodal peak around 4 nm can be seen in Fig. 3f for the pore size distribution, which further confirms the mesoporous structure of $CoFe_2O_4$ nanowire. The formation of the mesopores could be related to the gas release during the

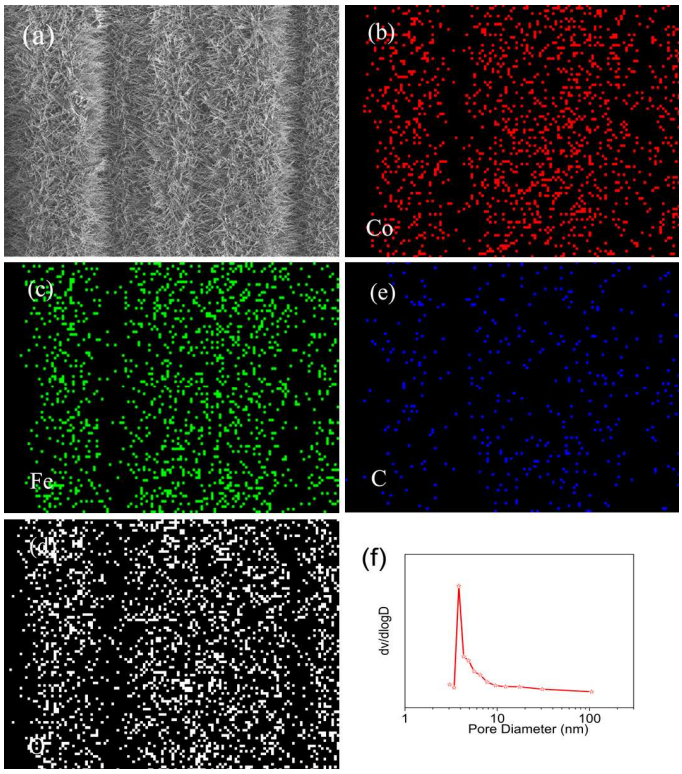

Fig. 3 (a) SEM image of $CoFe_2O_4$/carbon fabric composite; EDX elemental mappings of (b) cobalt, (c) iron, (d) oxygen, and (e) carbon. (f) The pore size distribution of $CoFe_2O_4$ naowires.

Physical Chemistry Chemical Physics Accepted Manuscript

This journal is © The Royal Society of Chemistry 2015

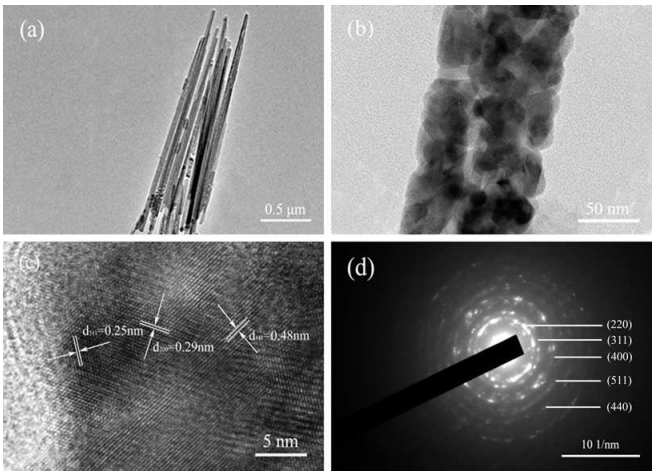

Fig. 4 (a,b) TEM, (c) HRTEM images, and d) SAED pattern of the $CoFe_2O_4$ naowires scratched down from the carbon fabric.

decomposition of the Co-Fe precursor.

To better illustrate the unique architecture and porous feature, representative TEM images of nanowires are given in Fig. 4. As shown in a low-magnification TEM image (Fig. 4a) of several $CoFe_2O_4$ nanowires. the needle-like $CoFe_2O_4$ nanowires with diameter 70-100 nm and length up to several micrometer can be clearly seen, which are in good agreement with the SEM observations. A higher-magnification TEM image depicted in Fig. 4b further reveals that a typical $CoFe_2O_4$ nanowire is actually a porous nanowire composed of many small nanoparticles of 15-20 nm in diameter instead of the conventional single-crystal nanowire. The mesopores structure enable facile penetration of the electrolyte to the surfaces of $CoFe_2O_4$, resulting in rapid charge transfer reactions due to the shorten ions diffusion paths. Fig. 4c demonstrates the HRTEM image of a single porous $CoFe_2O_4$ nanowire. The clearly resolved lattice fringes show an interplanar spacing of 0.25nm, 0.29nm and 0.48nm, corresponding to the (311) (200) and (111) planes of spinel $CoFe_2O_4$.[40] The selected-area electron diffraction (SAED) pattern of the $CoFe_2O_4$ nanowires (Fig. 4d) shows well-defined concentric diffraction rings from the centre can be assigned to the (220), (311), (400), (511) and (440) planes of cubic spinel $CoFe_2O_4$, which is consistent with the XRD results.[41-43]

In virtue of the robust mechanical adhesion and good electrical contact enabled by the direct growth of metal oxide nanostructures on the current collector, the $CoFe_2O_4$/carbon fabric composite was further tested as LIBs anodes. The electrochemical experiments were conducted in a two-electrode configuration with the as-prepared $CoFe_2O_4$/carbon fabric composite used directly as the working electrode without any insulating binder or conducting additive, and the results were compared with $CoFe_2O_4$ electrode made by the traditional slurry-coating technique. Fig. 5a displays the initial five consecutive cyclic voltammogram (CV) curves of $CoFe_2O_4$/carbon fabric electrode at a scan rate of 0.1 mV s^{-1} in the voltage window of 0.005-3.0 V. The first CV curve is obviously different from the following cycles and the following CV curves are almost overlapped from the second to the fifth cycle, presenting excellent reversible performances except for the irreversible reactivity in the first cycle. In the first cycle, there is an obvious irreversible reduction peak around 0.5 V, which can be assigned to Li intercalation into the lattice followed by $CoFe_2O_4$ crystal structure destruction and formation of the respective nanosize metal particles (reduction of $CoFe_2O_4$ to metallic Fe and Co), as well as the decomposition of organic electrolyte to form a solid-electrolyte interphase (SEI) layer at the electrode/electrolyte interphase.[44] In the anodic process, the broad peaks between 1.6 and 2.0 V can be ascribed to the multistep oxidation of metallic Fe and Co to their oxide states, which showed no obviously shift in the subsequent cycles.[18, 45-47] Meanwhile, the peak around 0.4 V is ascribed to the co-efficiency between the carbon fabric and the electrode material.[48] Besides, similar CV curves are obtained from $CoFe_2O_4$ powder pasted electrode (Fig. S5, see the Supporting Information), indicating the little influence of substrates on the electrochemical characteristics. Thus, on the basis of above CV analysis and the displacive redox mechanism of $CoFe_2O_4$ previous reported, the electrochemical reactions in the as prepared $CoFe_2O_4$/carbon fabric composite can be expressed as follows:[49, 50]

$$CoFe_2O_4 + 8Li^+ + 8e^- \rightarrow Co + 2Fe + 4Li_2O \quad (1)$$

$$Co + Li_2O \rightarrow CoO + 2Li^+ + 2e^- \quad (2)$$

$$2Fe + 3Li_2O \rightarrow Fe_2O_3 + 6Li^+ + 6e^- \quad (3)$$

$$Co + 2Fe + 4Li_2O \leftrightarrow CoO + Fe_2O_3 + 8Li^+ + 8e^- \quad (4)$$

During the following cycles, the reduction peak is moved to around 0.75 V and the oxidation peaks are almost unaltered. The slight shift of the reduction peak to higher potential in the

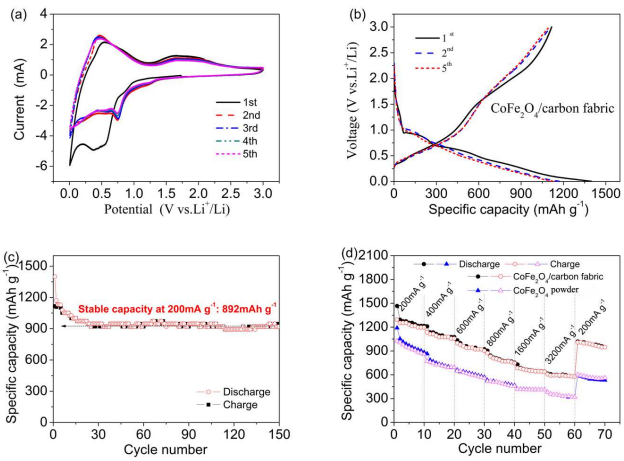

Fig. 5 (a) Cyclic voltammograms of the $CoFe_2O_4$/carbon fabric electrode for the initial five cycles at a scan rate of 0.1 mV s^{-1} in the voltage range of 0.005-3.0 V, (b) Charge-discharge voltage profiles of $CoFe_2O_4$/carbon fabric electrode for the first five cycles at a current density of 200 mA g^{-1}, (c) cycling performance of $CoFe_2O_4$/carbon fabric electrode at the current density of 200 mA g^{-1}, and (d) comparison of rate capability of $CoFe_2O_4$/carbon fabric electrode with $CoFe_2O_4$ powder pasted electrode.

Physical Chemistry Chemical Physics Accepted Manuscript

following cycles might be related to some activation process caused by the Li^+ insertion in the first cycle, indicating the slightly easier reduction in the subsequent cycles.[51,52]

The typical discharge-charge voltage profiles of $CoFe_2O_4$/carbon fabric electrode for the first five cycles at a current density of 200 mA g^{-1} in the range of 0.005 and 3.0 V are shown in Fig. 5b. Notably, these typical voltage plateaus match well with the peaks observed in the CV curves. Significantly, the $CoFe_2O_4$/carbon fabric electrode delivers high first-cycle discharge and charge capacities of 1398.74 and 1116.83 mAh g^{-1} respectively, corresponding to a moderate irreversible loss of about 20.15%. In addition to the large specific mass capacity, the $CoFe_2O_4$/carbon fabric electrode also have a large corresponding areal discharge capacity of ~1.78 mAh cm^{-2} at a current densities of 0.25 mA cm^{-2}. Such irreversible capacity loss during the first cycle can be commonly attributed to the decomposition of electrolyte and the formation of solid-electrolyte interphase film,[53] which is a common drawback for nanostructured anodes and requires further efforts to resolve this problem. Besides, the carbon textiles exhibit quite low capacity (Fig. S6, Supporting Information), indicating that the carbon fabric makes little contribution to the total specific capacity of the composite electrode.

As expected, the $CoFe_2O_4$/carbon fabric electrode manifests good cycling stability. The cycling performance of the $CoFe_2O_4$/carbon fabric electrode and $CoFe_2O_4$ powder pasted electrode is illustrated in Fig. 5c and Fig. S7 (Supporting Information). From the second cycle onwards, the discharge capacity of the $CoFe_2O_4$/carbon fabric electrode shows very slow fading. The reversible lithium storage capacity gradually becomes stable at ~950 mAh g^{-1} (corresponding areal capacity of ~1.21 mAh cm^{-2}) after about 50 cycles. There is no obvious capacity decay after experiencing 150 cycles. Interestingly, a reversible discharge capacity as high as 954.3 mAh g^{-1} (areal capacity of ~1.21 mAh cm^{-2}) is retained after 150 cycles, corresponding to 87.1% of the second-cycle discharge capacity, which is still much higher than the theoretical capacity value based on the conversion reaction (4). The similar phenomena can be commonly observed in a variety of metal oxides-based anodes due to the reversible growth of the electro-chemistry active polymeric gel-like film by the kinetically activated electrolyte degradation.[54-57] For the $CoFe_2O_4$/carbon fabric electrode, the excess capacity is associated with the reversible formation/dissolution of the polymeric surface layer, which in general contributes to additional capacity.[58-61] The polymeric surface layer, which is coated outside the inorganic SEI layer, is reported to show pseudocapacitive character and account for the origin of the low-voltage capacity.[61] Besides, the Coulombic efficiency rapidly increases to and stabilizes at around 98% after a few cycles, again confirming the excellent electrochemical reversibility of the electrode. Under the identical test conditions, $CoFe_2O_4$ powder pasted electrode exhibit much faster capacity fading, and a capacity of only around 540 mAh g^{-1} is left after 150 cycles at a current density of 200 mA g^{-1} as shown in Fig. S7b (Supporting Information).

Rate performance of $CoFe_2O_4$/carbon fabric integrated electrode and $CoFe_2O_4$ powder pasted electrode were compared at various current densities ranging from 200 to 3200 mA g^{-1}, as shown in Fig. 5d. The $CoFe_2O_4$ powder pasted electrode exhibits high initial discharge capacity, followed however by a sharp capacity decay with the increase of current density. However, the discharge capacity of $CoFe_2O_4$/carbon fabric electrode steadily decreases as the gradual increase of current density, with an average value of 1269.9, 1108.4, 954.2, 800.7, 663.6 595.3 and 985.9 mAh g^{-1} obtained at current density of 200, 400, 600, 800, 1600, 3200, and 200 mA g^{-1}, respectively. The corresponding areal discharge capacities are 1.61, 1.41, 1.21, 1.02, 0.84, 0.76 and 1.25 mAh cm^{-2}, respectively. It clearly reveals when the applied current density increases, the $CoFe_2O_4$/carbon fabric electrode shows gradual decreases of the discharge capacity, which is attributed to the increasing polarization of the electrodes at high current densities.[62,63] Apparently, $CoFe_2O_4$/carbon fabric integrated electrode, exhibits much higher lithium-ion storage capacity and much better rate capability than $CoFe_2O_4$ powder pasted electrode. For instance, even at a very high current density of 3200 mA g^{-1}, the capacity of $CoFe_2O_4$/carbon fabric electrode was higher than $CoFe_2O_4$ powder pasted electrode. Importantly, a high capacity of 1018.94 mAh g^{-1} can be recovered when the current density is reduced back to 200 mA g^{-1}, indicating excellent stability of the $CoFe_2O_4$/carbon fabric electrode. The second charge-discharge voltage profiles of $CoFe_2O_4$/carbon fabric electrode tested at different current densities is shown in Fig. S8 (Supporting Information). It is also noticed that the electrode polarization increases with decreasing reversible capacity as the current density increases. We also compared the $CoFe_2O_4$/carbon fabric electrode presented in this work with other $CoFe_2O_4$-based electrodes reported in recent literature, and the result shown in Table S1 (Supporting Information). The lithium storage capacity and rate performance of $CoFe_2O_4$/carbon fabric electrode are superior to most $CoFe_2O_4$ pasted electrodes. The significantly different electrochemical properties for the two typed electrodes are attributed to the different electrode architectures.

To the best of our knowledge, the mass and areal capacities displayed here is much higher than many previous

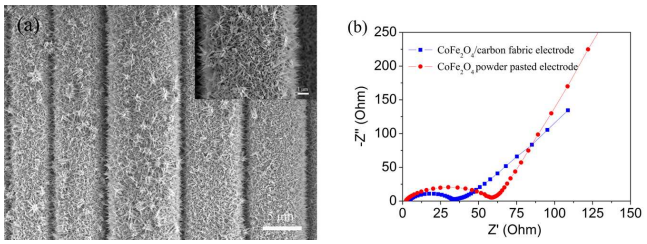

Fig. 6 (a) SEM images of the $CoFe_2O_4$/carbon fabric electrode after 100 cycles at a constant current density of 200 mA g^{-1} at different magnifications. (b) Nyquist plots of the $CoFe_2O_4$/carbon fabric and $CoFe_2O_4$ powder pasted electrodes measured with an amplitude of 5 mV over the frequency range of 100 kHz and 0.01 Hz.

Physical Chemistry Chemical Physics Accepted Manuscript

This journal is © The Royal Society of Chemistry 2015

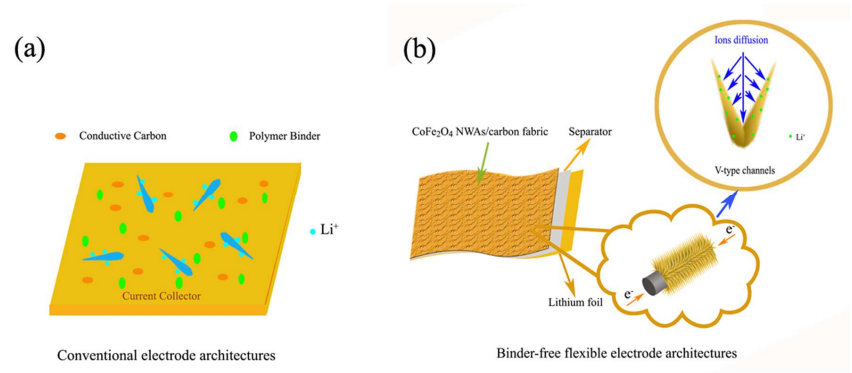

Fig. 7 Schematic drawing of a) the conventional $CoFe_2O_4$ powder pasted electrode and b) $CoFe_2O_4$/carbon fabric electrode.

reports, such as TiO_2@Fe_2O_3 nanowire array (first discharge capacity is ~800 mAh g^{-1} at a current density of 100 mA g^{-1}),[64] TiO_2 nanotubes (first discharge capacity is 0.678 mAh cm^{-2} and decreases to 0.2 mAh cm^{-2} after 45 cycles at current density of 0.025 mA cm^{-2}),[65] TiO_2@ZnO nanotube array (first discharge capacity is 0.427 mAh cm^{-2} and decreases to 0.17 mAh cm^{-2} after 200 cycles at current density of 0.05 mA cm^{-2}),[66] crystalline SnO_2 nanowire/TiO_2 nanotube (0.14 mAh cm^{-2} at 0.05 mA cm^{-2}).[67] Typically, the current densities in our experiment are much higher, while the mass and areal capacities and cyclability of our $CoFe_2O_4$ nanowire arrays are much better.

The morphology of the $CoFe_2O_4$/carbon fabric electrode was analyzed after 100 cycles by SEM as shown in Fig. 6a. The self-supported nanowire morphology was well retained after the cycling test, which is due to the good structural stability of the mesoporous $CoFe_2O_4$ nanowires. This result indicates that the $CoFe_2O_4$ nanowires arrays have good adhesion to the carbon fabric substrate and such 3D architecture is stable during the cycling test. Moreover, the nanowire became much thicker as shown in the inset of Fig. 6a.

The directly grown $CoFe_2O_4$/carbon fabric and $CoFe_2O_4$ powder pasted electrodes were also characterized by electrochemical impedance spectroscopy (EIS) to evaluate their susceptibility to structural degradation. The results, presented as Nyquist plots (as shown in Fig. 6b), show the usual feature of a depressed semicircle at high-medium frequency region and a slopping line at low frequency region. It is obvious that the size of the semicircle for the $CoFe_2O_4$ powder pasted electrode is much bigger than that of the $CoFe_2O_4$/carbon fabric electrode, indicating that the conventional binder-enriched electrode increase additional undesirable interparticle resistance, which failed to provide efficient electron transport between electroactive materials and current collector substrate (Fig. 7). The enhanced electrochemical properties of the $CoFe_2O_4$ NWAs/carbon fabric integrated electrode could be attributed to the rationally designed nanostructure and the integrated smart architecture. Specifically, the abundant mesoporous structure in nanowires and large open spaces between neighboring nanowires provide high electrode/electrolyte contact area and more "V-type" channels for high Li^+ ions diffusion, and sufficient free mesopores to accommodate the the strain induced by the volume change during continuous charge-discharge cycling, thus dramatically boosting the cyclability of LIBs. More importantly, the $CoFe_2O_4$ NWAs with direct adhesion to high electrical conductivity carbon fabric can facilitate electron transport between the charge collecting substrates of carbon fabric and the every $CoFe_2O_4$ naowires, ultimately reducing internal resistance and enhancing the rate performance of LIBs. Together with the robust integrated architecture, high specific capacity, remarkable cycling stability and rate capability, the $CoFe_2O_4$ NWAs/carbon fabric is able to manifest excellent reversible lithium storage properties.

Conclusions

In summary, mesoporous $CoFe_2O_4$ NWAs were successfully grown on carbon textiles substrates with robust adhesion via a simple hydrothermal method process followed by a post-annealing treatment. Compared to traditional nanostructure powder pasted electrodes, directly grown nanostructure array electrodes not only simplify the conventional tedious process of electrode, but also offer remarkable advantages such as fast electron transport/collection and ion diffusion, sufficient electrochemical reaction of individual nanostructures, enhanced material-electrolyte contact area and facile accommodation of the strains caused by lithium intercalation and de-intercalation. When evaluated as binder-free anode materials for LIBs, the $CoFe_2O_4$/carbon fabric composite demonstrates a high reversible capacities of 1185.75 mAh g^{-1} at a current density of 200 mA g^{-1}, retaining 954.3 mAh g^{-1} after 150 cycles, and high rate capability. More importantly, the electrode design concept proposed in present work will provide new insight into the design and synthesis of other mesoporous transition metal oxides NWAs on flexible conductive substrate for the fabrication of high-performance flexible energy storage devices.

Physical Chemistry Chemical Physics Accepted Manuscript

Acknowledgements

This work was financially supported by the National Natural Science Foundation of China (Grant No. 51271012) and Innovation Foundation of Beihang University for PhD Graduates. The authors thank the Analysis and Testing Center of the School of Materials Science and Engineering of Beihang University for support.

Notes and references

1 J. R. Miller, and P. Simon, *Science,* 2008, **321,** 651.
2 X. Li, X. B. Zang, Z. Li, X. M. Li, P. X. Li, P. Z. Sun, X. Lee, R. J. Zhang, Z. H. Huang, K. L. Wang, D. H. Wu, F. Y. Kang, and H. W. Zhu, *Adv. Funct. Mater.,* 2013, **23,** 4862.
3 X. H. Lu, T. Zhai, X. H. Zhang, Y. Q. Shen, L. Y. Yuan, B. Hu, L. Gong, J. Chen, Y. H. Gao, J. Zhou, Y. X. Tong, and Z. L. Wang, *Adv. Mater.,* 2012, **24,** 938.
4 M. Armand, and J. -M. Tarascon, *Nature,* 2008, **451,** 652.
5 D. Zhou, H. Wu, Z. Wei, and B. -H. Han, *Phys. Chem. Chem. Phys.,* 2013, **15,** 16898-16906.
6 G. M. Zhou, F. Li, and H. M. Cheng, *Energy Environ. Sci.,* 2014, **7,** 1307.
7 L. Li, Z. Wu, S. Yuan, and X. B. Zhang, *Energy Environ. Sci.,* 2014, **7,** 2101.
8 H. H. Cheng, Z. L. Dong, C. G. Hu, Y. Zhao, Y. Hu, L. T. Qu, N. Chen, and L. M. Dai, *Nanoscale,* 2013, **5,** 3428.
9 X. H. Lu, M. H. Yu, G. M. Wang, Y. X. Tong, and Y. Li, *Energy Environ. Sci.,* 2014, **7,** 2160.
10 K. Jost, C. R. Perez, J. K. McDonough, V. Presser, M. Heon, G. Dion, and Y. Gogotsi, *Energy Environ. Sci.,* 2011, **4,** 5060.
11 X. Xiao, T. P. Ding, L. Y. Yuan, Y. Q. Shen, Q. Z. Zhong, X. H. Zhang, Y. Z. Cao, B. Hu, T. Zhai, L. Gong, J. Chen, Y. X. Tong, J. Zhou, and Z. L. Wang, *Adv. Energy. Mater.,* 2012, **2,** 1328.
12 P. P. Yu, Y. Z. Li, X. Zhao, L. H. Wu, and Q. H. Zhang, *Langmuir,* 2014, **30,** 5306.
13 L. B. Hu, M. Pasta, F. L. Mantia, L. F. Cui, S. Jeong, H. D. Deshazer, J. W. Choi, S. M. Han, and Y. Cui, *Nano Lett.,* 2010, **10,** 708.
14 J. Du, G. Zhou, H. M. Zhang, C. Cheng, J. M. Ma, W, F. Wei, L. B. Chen, and T. H. Wang, *ACS Appl. Mater. Interfaces.,* 2013, **5,** 7405.
15 M. H. Yu, T. Zhai, X. H. Lu, X. J. Chen, S. L. Xie, W. Li, C. L. Liang, W. X. Zhao, L. P. Zhang, and Y. X. Tong, *J. Power Sources,* 2013, **239,** 64.
16 G. X. Gao, H. B. Wu, and X. W. Lou, *Adv. Energy Mater.,* 2014, **4,** 1400422.
17 B. Wang, S. M. Li, J. H. Liu, M. Yu, B. Li, and X. Y. Wu, *Electrochim. Acta,* 2014, **146,** 679.
18 Y. Xiao, J. Zai, L. Tao, B. Li, Q. Han, C. Yu, and X. Qian, *Phys. Chem. Chem. Phys.,* 2013, **15,** 3939.
19 S. H. Ren, X. Y. Zhao, R. Y. Chen, and M. Fichtner, *J. Power Sources,* 2014, **260,** 205.
20 Z. L. Zhang, Y. H. Wang, M. J. Zhang, Q. Q. Tan, X. Lv, Z. Y. Zhong, and F. B. Su, *J. Mater. Chem. A.,* 2013, **1,** 7444.
21 X. N. Fu, D. Chen, M. Wang, Y. S. Yang, Q. Z. Wu, J. M. Ma, and X. S. Zhao, *Electrochim. Acta,* 2014, **116,** 164.
22 L. Zhang, H. B. Wu, and X. W. Lou, *Adv. Energy Mater.,* 2014, **4,** 1300958.
23 S. Y. Liu, J. Xie, C. C. Fang, G. S. Cao, T. J. Zhu, and X. B. Zhao, *J. Mater. Chem.,* 2012, **22,** 19738.
24 J. Gao, M. A. Lowe, and H. D. Abruna, *Chem. Mater.,* 2011, **23,** 3223.
25 J. Yan, A. Sumboja, E. Khoo, and P. S. Lee, *Adv. Mater.,* 2011, **23,** 746.
26 W. Q. Zeng, F. P. Zheng, R. Z. Li, Y. Zhan, Y. Y. Li, and J. P. Liu, *Nanoscale,* 2012, **4,** 2760.
27 J. Jiang, Y. Y. Li, J. P. Liu, and X. T. Huang, *Nanoscale,* 2011, **3,** 45.
28 W. Wang, M. Tian, A. Abdulagatov, S. M. George, Y. -C. Lee, and R. Yang, *Nano Lett.,* 2012, **12,** 655.
29 C. K. Chan, X. F. Zhang, and Y. Cui, *Nano Lett.,* 2008, **8,** 307.
30 Z. Sun, W. Ai, J. Liu, X. Qi, Y. Wang, J. Zhu, H. Zhang, and T. Yu, *Nanoscale,* 2014, **6,** 6563.
31 X. J. Lin, Y. S. Shang, T. Huang, and A. Yu, *Nanoscale,* 2014, **6,** 9043.
32 L. F. Shen, Q. Che, H. S. Li, and X. G. Zhang, *Adv. Funct. Mater.,* 2014, **24,** 2630.
33 H. Xia, D. D. Zhu, Y. S. Fu, and X. Wang, *Electrochim. Acta,* 2012, **83,** 166.
34 P. Jing, L. Pan, J. Du, J. Wang, and Q. Liu, *Phys. Chem. Chem. Phys.,* 2015, **17,** 12841.
35 M. Zhang, X. Yang, X. F. Kan, X. Wang, L. Ma, and M. Q. Jia, *Electrochim. Acta,* 2013, **112,** 727.
36 J. Li, S. Xiong, X. Li, and Y. Qian, *Nanoscale,* 2013, **5,** 2045.
37 Y. Hou, X. -Y. Li, Q. -D. Zhao, X. Quan, and G. -H. Chen, *Adv. Funct. Mater.,* 2010, **20,** 2165.
38 C. Altavilla, E. Ciliberto, A. Aiello, C. Sangregorio, and D. Gatteschi, *Chem. Mater.,* 2007, **19,** 5980.
39 X. F. Lu, L. Yang, X. J. Bian, D. M. Chao, and C. Wang, *Part. Part. Syst. Charact.,* 2014, **31,** 245.
40 Y. J. Yao, Z. H. Yang, D. W. Zhang, W. C. Peng, H. Q. Sun, and S. B. Wang, *Ind. Eng. Chem. Res.,* 2012, **51,** 6044.
41 Y. J. Xu, W. Y. Bian, J. Wu, J. -H. Tian, and R. Z. Yang, *Electrochim. Acta,* 2015, **151,** 276.
42 W. Y. Bian, Z. R. Yang, P. Strasser, and R. Z. Yang, *J. Power Sources,* 2014, **250,** 196.
43 P. R. Kumar, P. Kollu, C. Santhosh, K. E. V. Rao, D. K. Kim, and A. N. Grace, *New J. Chem.,* 2014, **38,** 3654.
44 S. G. Mohamed, T. -F. Hung, C. -J. Chen, C. K. Chen, S. -F. Hu, R. -S. Liu, K. -C. Wang, X. -K. Xing, H. -M. Liu, A. -S. Liu, M. -H. Hsieh, and B. -J. Lee, *RSC Adv.,* 2013, **3,** 20143.
45 Y. Ding, Y. F. Yang, and H. X. Shao, *J. Power Sources,* 2013, **244,** 610.
46 L. Y. Wang, L. H. Zhuo, C. Zhang, and F. Y. Zhao, *J. Power Sources,* 2015, **275,** 650.
47 Y. L. Xiao, J. T. Zai, X. M. Li, Y. Gong, B. Li, Q. Y. Han, and X. F. Qian, *Nano Energy,* 2014, **6,** 51.
48 X. J. Hou, X. F. Wang, B. Liu, Q. F. Wang, T. Luo, D. Chen, and G.Z. Shen, *Nanoscale,* 2014, **6,** 8858.
49 P. Poizot, S. Laruelle, S. Grugeon, L. Dupont, J. -M. Tarascon, *Nature,* 2000, **407,** 496.
50 P. Lavela, and J. L. Tirado, *J. Power Sources,* 2007, **172,** 379.

Physical Chemistry Chemical Physics Accepted Manuscript

 This journal is © The Royal Society of Chemistry 2015

51 L. Zhou, D. Y. Zhao and X. W. Lou, *Adv. Mater.,* 2012, **24,** 745.
52 G. N. Zhu, Y. G. Wang and Y. Y. Xia, *Energy Environ. Sci.,* 2012, **5,** 6652.
53 L. L. Li, H. B. Wu, L. Yu, S. Madhavi, and X.W. Lou, *Adv. Mater. Interfaces.,* 2014, **1,** 1400050.
54 G. M. Zhou, D. W. Wang, F. Li, L. L. Zhang, N. Li, Z. S. Wu, L. Wen, G. Q. Lu, and H. M. Cheng, *Chem. Mater.,* 2010, **22,** 5306.
55 F. M. Courtel, H. Duncan, Y. Abu-Lebdeh, and I. J. Davidson, *J. Mater. Chem.,* 2011, **21,** 10206.
56 G. Q. Zhang, L. Yu, H. B. Wu, H. E. Hoster, and X. W. Lou, *Adv. Mater.,* 2012, **24,** 4609.
57 K. M. Shaju, F. Jiao, A. Debart, and P. G. Bruce, Phys. *Chem. Chem. Phys.* 2007, **9,** 1837.
58 H. Fang, S. C. Zhang, W. B. Liu, Z. J. Du, X. M. Wu, and Y. L. Xing, *Electrochim. Acta,* 2013, **108,** 651.
59 Z. Wang, D. Luan, S. Madhavi, Y. Hu, and X. W. Lou, *Energy Environ. Sci.,* 2012, **5,** 5252.
60 C. Ban, Z. Wu, D. T. Gillaspie, L. Chen, Y. Yan, J. L. Blackburn, and A. C. Dillon, *Adv. Mater.,* 2010, **22,** E145.
61 C. Li, X. Yin, L. Chen, Q. Li, and T. Wang, *Chem.-Eur. J.,* 2010, **16,** 5215.
62 K. Karthikeyan, S. Amaresh, G. W. Lee, V. Aravindan, H. Kim, K. S. Kang, W. S. Kim, and Y. S. Lee, *Electrochim. Acta,* 2012, **68,** 246.
63 J. Lu, Y. -L. Chang, B. Song, H. Xia, J. -R. Yang, K. S. Lee, and L. Lu, *J. Power Sources,* 2014, **271,** 604.
64 H. Xia, W. Xiong, C. K. Lim, Q. F. Yao, Y. D. Wang, and J. P. Xie, *Nano. Res.,* 2014, **7,** 1797,
65 G. F. Ortiz, I. Hanzu, P. Lavela, J. L. Tirado, P. Knauth, and T. Djenizian, *J. Mater. Chem.,* 2010, **20,** 4041.
66 R. Li, Z. Xie, H. Lu, D. W. Zhang, and A. Yu, *Int. J. Electrochem. Sci.,* 2013, **8,** 11118.
67 G. F. Ortiz, I. Hanzu, P. Lavela, P. Knauth, J. L. Tirado, and T. Djeniziana, *Chem. Mater.,* 2010, **22,** 1926.

Physical Chemistry Chemical Physics Accepted Manuscript